

PROPERTIES OF ULTRA HIGH PERFORMANCE CONCRETE (UHPC) IN TENSION AT HIGH STRAIN RATES

MARKUS NÖLDGEN^{*}, WERNER RIEDEL[†], KLAUS THOMA[†] AND EKKEHARD FEHLING[†]

^{*} Cologne University of Applied Sciences
Professor for Reinforced Concrete Structures and Statics
Betzdorfer Str. 2, 50679 Cologne, Germany
e-mail: markus.noeldgen@fh-koeln.de, web page: <http://www.f06.fh-koeln.de/>

[†] Fraunhofer Institute for High-Speed Dynamics
‘University of Kassel, Chair of Reinforced Concrete

Key words: Ultra-High-Performance Concrete, Strain Rate in Tension, Fracture Energy, Stress-Crack Opening Relation, Hopkinson-Bar and Impact Experiments

Abstract: This paper is a contribution to the material description of Ultra High Performance Concrete (UHPC) at high-speed dynamic loading conditions. Based on a series of Hopkinson-Bar experiments, dynamical material parameters such as the Tensile Strength, Young’s Modulus and Fracture Energy are determined at high strain rates of 10^2 s^{-1} . A comparison with the results of these parameters for normal and high strength concretes leads to a qualitative and quantitative description of UHPC at high strain rates. Differences in macroscopic strain-rate-effects occur due to a significantly reduced amount of the moisture effect (reduced capillary pores) on the one side and a different relation of aggregate to grout strength for UHPC on the other side (section 1).

Based on the experimentally determined Fracture Energy and Stress-Crack-Opening-Relation a material model for UHPC at high strain-rates is postulated by extending the established RHT concrete damage model with a new fracture mechanical damage law (section 2). Numerical hydrocode simulations of the Hopkinson-Bar Experiments are presented to proof the evidence of the concrete model for a one-dimensional wave propagation problem. Furthermore a series of impact experiments on rebar reinforced UHPC plates with more complex three-dimensional wave propagation show a satisfying accuracy of the new fracture mechanic concrete model even for more complex failure mechanisms from cracking of the concrete to perforation of aircraft engine missiles at high strain rates (section 3).

1. EXPERIMENTS ON UHPC AT HIGH STRAIN RATES IN TENSION

There is currently no experimentally substantiated basis available for the strength description of the material UHPC under high-speed dynamic loading. For normal-strength concrete, in contrast, there are numerous experimental results and mechanical models [1-10]. Further authors [11-14] have

investigated high-strength and normal-strength fiber reinforced concretes with varied fiber contents. The strain-rate-dependent strength increase is often applied as a ratio of the dynamic to static strength and described internationally as “dynamic increase factor, DIF”. Figure 1 shows experimentally determined values for the strain-rate-dependent tension strength of normal-strength concrete. All the experiments carried out have

in common a significant and from $\dot{\epsilon} \geq 1 \text{ s}^{-1}$ over-proportionally increasing effect of strain rate on the tension strength which is dedicated to a limited crack-opening velocity in the evolution of cracks [1,15]. An analogous conclusion from normal concrete to UHPC is, however, not possible without further experimental data, because significant differences have already been determined for high-strength concretes [1,16-19].

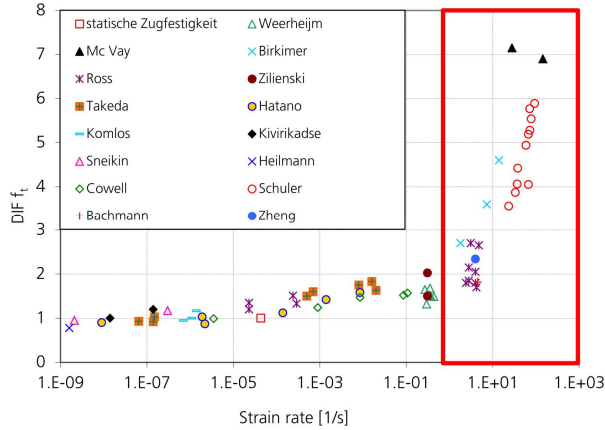


Figure 1: Dynamic increase factor (DIF f_t) for the tension strength of various concretes [20]

Lok [13] and Schuler [19] investigate the influence of increasing compression strength and the fibers [11,13,14] on the dynamic tension-bearing properties of high-strength concrete through the use of Hopkinson-bar spallation experiments under strain rates of 10^1 to 10^2 s^{-1} . The results are shown in Figure 2.

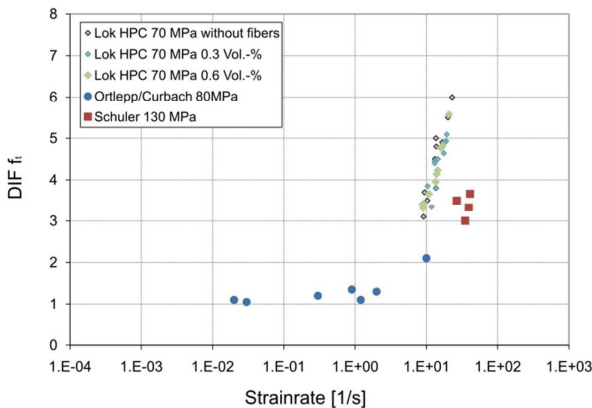


Figure 2: Dynamic Increase Factor (DIF f_t) for the tension strength of various high-strength concretes [20]

Possible causes for the observed strain-rate-dependent strength behavior of high-strength and ultra-high-strength concretes can be described with the following hypotheses:

- With the alterations to the material composition, the essential failure mechanism changes. Instead of the failure of the contact surface of matrix and aggregate, the aggregate grains themselves increasingly fail. This effect, which is given in [1] as one of the causes for the strength increase for normal concretes, already occurs in high-strength concretes under static conditions, and therefore does not lead to a further increase of strength under higher loading velocities. Proof of this is delivered by Ortlepp in [18]. His fractal analyses show the considerably altered failure surface in comparison to normal concrete and point to another, more finely distributed cracking behavior.
- The tension strength-increasing effect of pore water described by Rossi et al. [22,23] and Ross et al. [6], called the Stefan effect, reduces with the reduced porosity in high-strength concretes (see Figure 3).

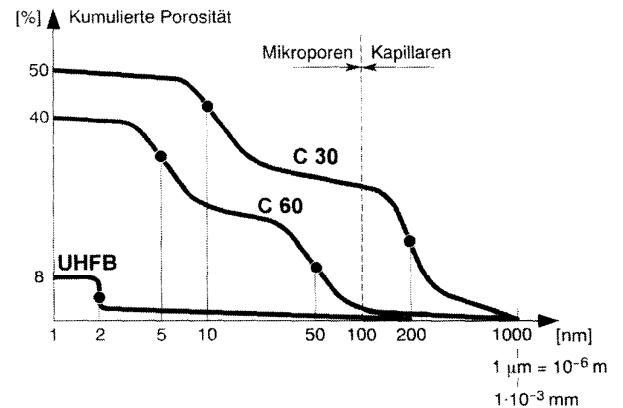


Figure 3: Porosity of C30/C60 and UHFB mixture [21]

- Inertia effects in crack evolution which determine the second step increase in the DIF are driven by tension failure mechanism in fibrous materials. The crack process is presumably determined by the fiber bond and fiber failure strength rather than aggregate interlock effects in plain concrete.

Experimental program – Static Tests

For a reference UHPC-mixture, static experiments are performed to determine the uniaxial compression strength, uniaxial tension strength, Young's modulus and fracture energy. The mixture recipes used for UHPC are B4Q and B5Q [24]. The fiber content in

the UHPC-mixture varies between 1.0 % vol. and 2.5 % vol. The fibers used are micro-fibers with an l/d ratio of 9 mm/ 0.15 mm, for which extensive static investigations with UHPC are available for reference [24,25,26]. To determine the influence of the fibers, a reference mixture without fibers is also used.

In order to make the results as comparable as possible, specimens are made from one mix with 0 % vol., 1.0 % vol. and 2.5 % vol. Cubes, cylinders and prisms are formed individually. The Hopkinson-bar cylinders are drilled out of a panel with dimensions of 600/600/320 mm as drill cores. In order to reduce the influence of the aligned fiber orientation at the base of the formwork, the ends of the drill core are shortened by 35 mm at each end and ground parallel (Figure 4).

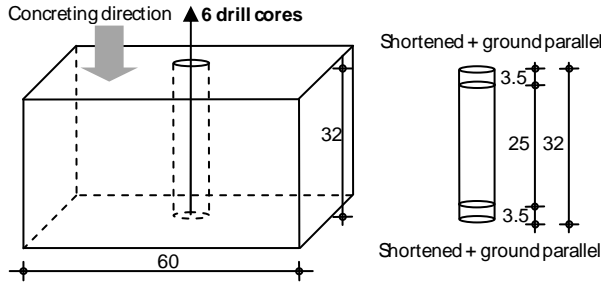


Figure 4: Drill core removal for specimen for the Hopkinson-bar experiments taken from the central section of a conventionally cast UHPC panel to avoid edge influence [20]

The cube compression strength increases considerably with increasing fiber content. The increase of strength due to the fibers of 15 % at 2.5 % vol. fiber content, which was observed by Fehling [24], is exceeded. This effect can also be observed in the cylinder compression strength experiments, where the average compression strength of the reference mix without fibers is 152.9 N/mm², with 1 % vol. fibers 173.3 N/mm² and with 2.5 % vol. fibers 208.1 N/mm².

The tension strength increases from 6.0 N/mm² to 6.6 N/mm² with 1 % vol. fiber content and to 9.4 N/mm² with 2.5 % vol. fiber content. In this case, the matrix tension strength defines the fracture state at a fiber content of 0 % vol. or 1 % vol., respectively, while at a fiber content of 2.5 % vol., the fiber effectiveness leads to a further increase of load

and thus to a higher fracture stress. The observation by Leutbecher [25], that strengthening behavior due to the fiber using short micro-fibers 9 mm/0.15 mm only occurs at fiber contents of more than 1 % vol., could be confirmed in the tension experiments.

Figure 5 shows an example of an experimentally determined stress-crack opening relationship against the calculation law according to Leutbecher [25]. The experimental results can be repeated as a good approximation with the aid of Equations (1) and (2).

$$\sigma = f_t \cdot \left(1 - \frac{w}{w_{\max}}\right)^2 \quad (1)$$

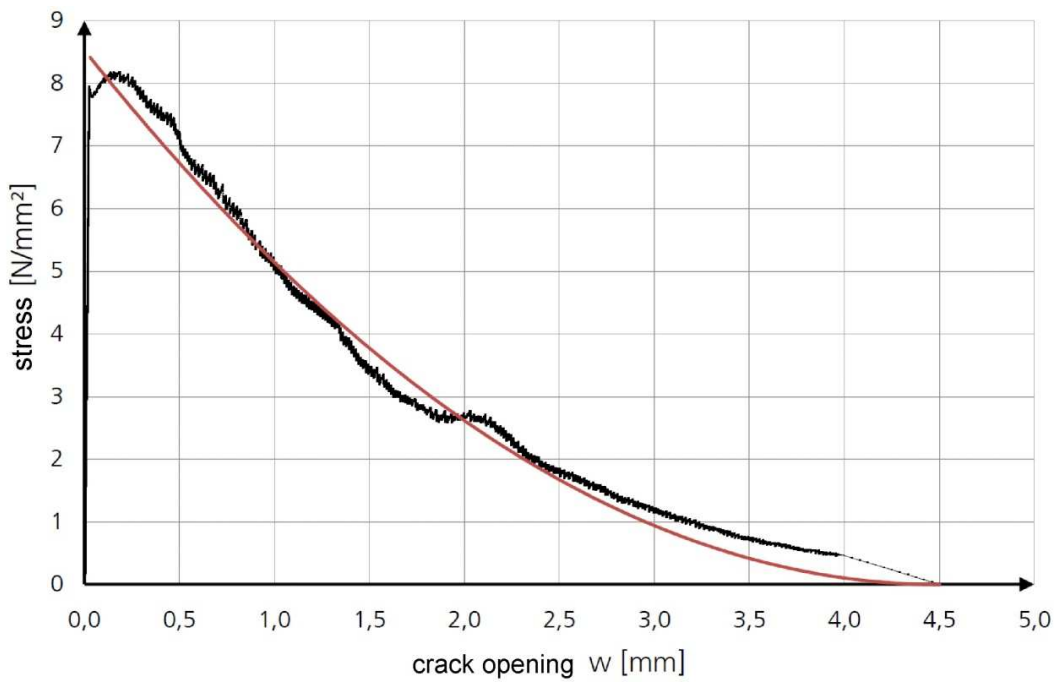
$$f_t = \eta \cdot g \cdot \rho_f \cdot \frac{\tau_{fm} \cdot l_f}{d_f} \quad (2)$$

The initial parameters used in Equation 1 are shown and explained in Table 1. The fiber pull-out from the UHPC is dependent on the fiber content ρ_f , on the bond between fiber and UHPC matrix expressed through the bonding stress τ_f and the surface of the fiber (l_f and d_f) and the Young's modulus of the fibers E_f . The achievable fiber effectiveness is dominated by the sample-specific fiber-orientation coefficient η and the fiber effectiveness coefficient g .

The fracture energy corresponds to the area under the stress-crack opening curve in Figure 5. It can be obtained directly by the summation of the stress increments from the direct tension tests. The values lie according to expectations about two orders of magnitude over the values for normal concrete (without fibers) and increase again considerably with increasing fiber content from 10,290 N/m to 13,935 N/m.

Table 1: Values for the calculated determination of the softening curve for UHPC [28]

	Value	Unit
Fiber content ρ_f	2.5	[% vol.]
Young's modulus of fibers E_f	200,000	[N/mm ²]
Bonding stress of fibers τ_f	11	[N/mm ²]
Diameter d_f	0.15	[mm]
Length l_f	9	[mm]
Fiber orientation coefficient η	0.771	[-]
Fiber effectiveness coefficient g	1	[-]
Fracture surface A_{Riss}	1028	[mm ²]

**Figure 5:** Example of a stress-crack opening relationship in the experiment with 2.5 % vol. fibers (black) in comparison with the calculated softening curve according to Equations (1), (2) (red). [28]

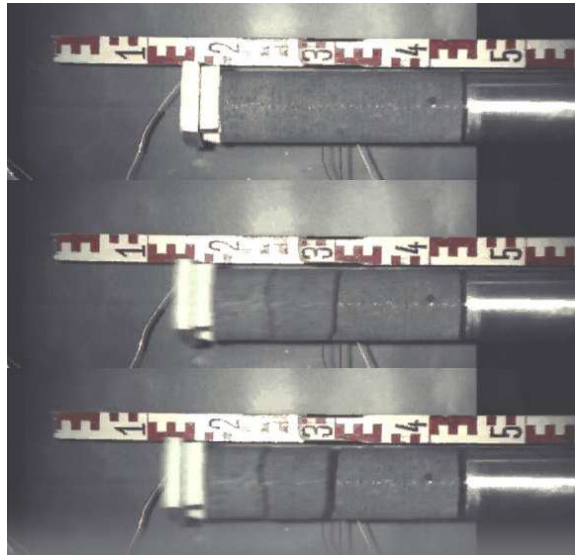


Figure 6: Sequence of pictures of a UHPC specimen for strength determination in the Hopkinson-bar spallation experiment. [28]

Table 2: Results from the Split-Hopkinson-Bar Experiments for UHPC for tension strength [28]

No.	ρ_f	$f_{c,stat}$	$f_{t,stat}$	$f_{t,dyn}$	Strainrate	DIF_{ft}	DIF_{ft}	Deviation CEB/Exp.
[-]	[Vol.-%]	[MN/m ²]	[MN/m ²]	[MN/m ²]	[1/s]	Experiment	CEB-FIP 90	[%]
1	0	152,9	8,6	41,1	103	4,8	5,2	9
2	0	152,9	8,6	38,5	114	4,5	5,4	21
3	0	152,9	8,6	46,2	122	5,4	5,6	3
4	0	152,9	8,6	40,6	103	4,7	5,2	11
5	0	152,9	8,6	39,1	114	4,6	5,4	19
6	0	152,9	8,6	38,9	111	4,5	5,4	19
7	1	173,3	9,3	41,8	111	4,5	5,3	18
8	1	173,3	9,3	47,2	164	5,1	6,0	19
9	1	173,3	9,3	39,1	115	4,2	5,4	28
10	1	173,3	9,3	42,9	129	4,6	5,6	21
11	2,5	208,1	10,5	51,2	132	4,9	5,5	14
12	2,5	208,1	10,5	53,8	148	5,1	5,7	12
13	2,5	208,1	10,5	60,9	156	5,8	5,9	2

Table 3: Results from the Split-Hopkinson-Bar Experiments for UHPC (Mean Values) [28]

	Dyn. Young's Modulus	Dyn. Tensile Strength	Dyn. Fracture Energy (specific)
Mixture, Fibres/Unit	[N/mm ²]	[N/mm ²]	[N/m]
B4Q 0,0 Vol.-%	50600	40,7	-
B4Q 1,0 Vol.-%	53100	42,7	10070
B5Q 2,5 Vol.-%	56600	55,3	11290

Hopkinson-Bar Spallation Experiments

The dynamic material experiments performed with UHPC samples are described as spallation experiments [3, 29, 7, 19]. This method can be used to determine the dynamic tension strength, the dynamic Young's modulus and the dynamic fracture energy. The experimental configuration is according to Schuler and his work should be referred to for the detailed description of the method and the evaluation scheme (Example of an experiment see Figure 6).

The strength increase under dynamic loading is given by the dimensionless dynamic load increase factor DIF (dynamic increase factor) as a function of the strain rate.

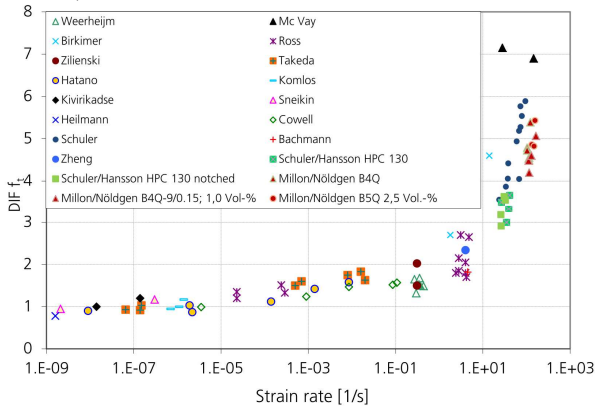


Figure 7: Dynamic Increase Factor (DIF_{f_t}) for the tension strength of different concretes and UHPC in comparison [19,28]

With the increase of strain rate, the strength under tension loading also increases significantly. The increase is less pronounced with increasing concrete strength. (Fig. 7,8)

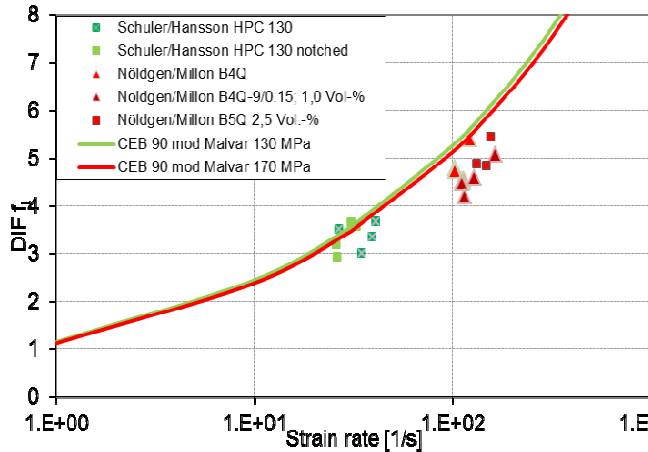


Figure 8: DIF_{f_t} for UHPC specimens compared to the

experiments of other authors on high-strength concretes and regression according to modified CEB law [28,30]

The calculation method according to Malvar et al. [31], which is used for example in [30], allows for the consideration of the concrete compression strength class, but shows an overestimation of the calculated value for experiments with UHPC in the strain rate zone of $\dot{\epsilon} \approx 100 \text{ s}^{-1} - 150 \text{ s}^{-1}$. The increase of tension strength is overestimated by an average of 15 % with values of 5.2 to 5.9 compared to the experimental values of 4.2 to 5.8. Table 2 shows the strength overestimation for all the individual results of the performed experimental series, as absolute values and as percentages. The initially formulated hypotheses about the behavior of UHPC under high strain rates can be indirectly confirmed by the results and are now evaluated individually using experimental observations. In addition to these values, the fracture surfaces are analyzed with optical and light microscopic pictures in order to be able to draw more conclusions about the failure behavior.

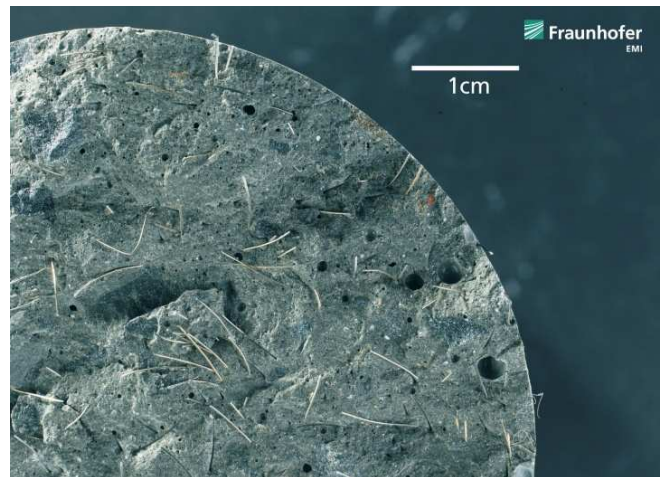


Figure 9: Fracture surface of UHPC after spallation [28]

- The fracture surface runs through the matrix and the aggregate grains in equal measure. Bypassing, i.e. failure in the contact zone between aggregate and matrix, as is

observed with normal concrete, does not occur. A strength increase under dynamic loading based on this effect cannot therefore be assumed mechanically. This observation agrees with the observations of [18] and [19] on high-strength concrete.

- The low porosity reduces the influence of the so-called Stefan effect on the dynamic strength increase (Figure 3). With the lower porosity, the influence of the cohesive effect of the free pore water reduces and thus reduces the strength increase under rapid loading.

Two essential hypotheses described in section 1 for a different strength and fracture behavior can be qualitatively confirmed through the experimental series. Based on the observations of other authors [6,10,18,22,23], it can be shown that the material properties of UHPC (reduced porosity, changed failure mechanism) tend to reduce the dynamic strength increase. The inertia effects in crack evolution however still dominate the DIF in the experimentally examined strain rate regime. The situation is illustrated in Figure 10. It should be noted that this macroscopic observation should be handled carefully in material models to avoid doubling of considered inertia effects (e.g. in dynamic calculations).

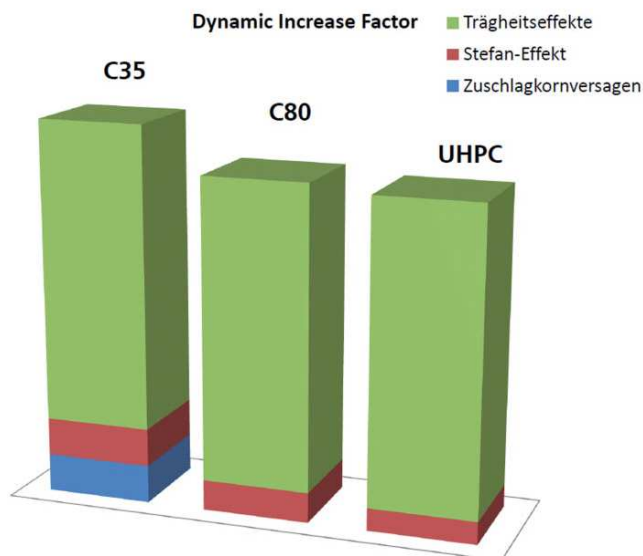


Figure 10: Causes of the strain rate effect DIF_{f_t} with increasing matrix strength and simultaneously reducing porosity (Stefan effect) [28]

To analyze the influence of the fibers on the tension-bearing behavior, the experimental results for UHPC are compared with other experimental results [11-14] on concretes with variable fiber content. An analysis of the fracture surface regarding the dominant fiber failure delivers further information about the contribution of the fibers to the load increase under strain rate influence. Using light microscope analyses, it was possible to demonstrate that the failure of the bond between fiber and matrix is decisive. Fiber cross-sections reduced through plastic deformation were not observed.

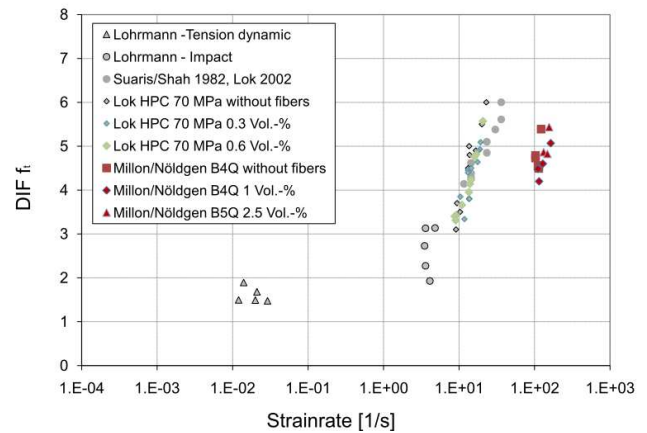


Figure 11: DIF_{f_t} for UHPC specimen in comparison to experiments from other authors with fiber concretes [28]

If the results for UHPC are compared with the results from other authors for fiber concrete, then this also shows a significant DIF for all configurations (Figure 11). With increasing fiber content, the dynamic tension strength also increases considerably (41 N/mm² to 53 N/mm²), so that the strain rate influence, as suspected, is present in the same way for the tension strength. At the same time, however, it is also noticeable that there is clearly no additional over-proportional increase of DIF between the UHPC specimen with and without fibers, as observed, for example, by Lok [12,13].

Dynamic fracture energy

The static fracture energy increases considerably with increasing fiber content from 10,290 N/m to 13,935 N/m. The dynamic

fracture energy also reaches values of 10,070 N/m and 11,290 N/m. Considering the relatively small number of samples, no tendency for the strain rate effect is clearly identifiable. Further experiments, which are being carried out in a parallel project at the Fraunhofer EMI, should deliver information about this tendency and its possible mechanical causes.

Dynamic softening hypothesis

The softening curve for fiber-reinforced UHPC cannot be directly measured from the spallation experiments. Nonetheless, a functional relationship can be proposed indirectly using the measured values and the known physical mechanisms, making use of the following constraints:

- i. $E_{\text{dyn}} \sim E_{\text{stat}}$ (Table 3). → The increase of the stress-strain relationship in the elastic zone has the same gradient under dynamic loading as under static conditions.
- ii. At high strain rates, the dynamic tension strength of the material increases (Tables 2, 3). → The strain rate effect observed with normal- and high-strength concretes also occurs with UHPC. A distinction between matrix tension strength and fiber effectiveness is not undertaken for the proposed softening hypothesis.
- iii. The fibers are pulled out of the matrix, no fiber tearing is observed (Figure 9). → The bonding stress determines the softening behavior as the governing parameter. This conclusion implies that the end point of the softening curve, as with static experiments at $w_{\text{max}} = l_f/2$, must be reached on the abscissa.
- iv. The dynamic fracture energy corresponds approximately to the static fracture energy for fiber UHPC. → Together with the already described observations, the dynamic softening curve lies only slightly below the static

softening curve and thus approximately congruent. A further proof of this important final conclusion is the experimental results from Pedersen et al. [10,32], which demonstrate the congruence of the static and dynamic softening curves at comparable strain rates of approx. $d\epsilon/dt = 10^2$ for normal concrete in similar form.

The resulting curve of the thus postulated softening curve is shown in Figure 12 as a synthesis of i. to iv. It is used in the material model for UHPC, described in Section 2.

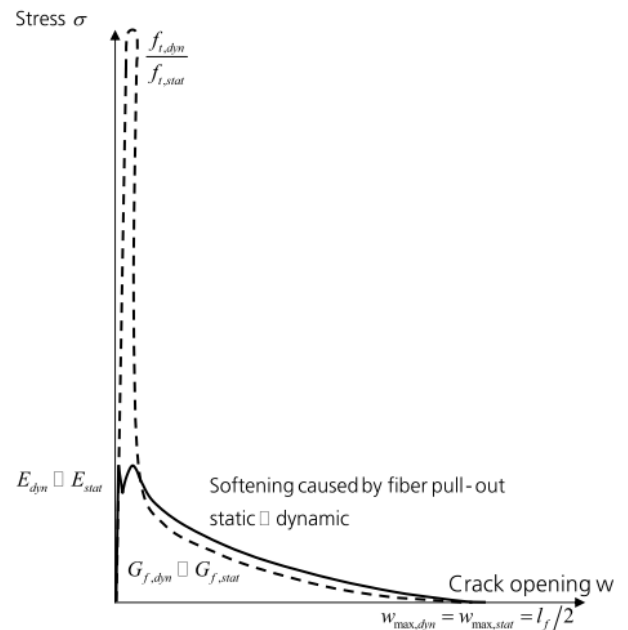


Figure 12: Illustration of the synthesis to the curve of the softening function for UHPC under dynamic loading (dashed curve) [28]

The link between the experimental stress-crack opening relationship and the plastic cracking strain increments resulting from the finite element calculations is made through the coupling in the damage description via Equations (1) and (2).

2. EXTENDED CONSTITUTIVE MODEL FOR UHPC

When wave propagation specific and large distortions are dominating the structural response at high-speed dynamic loading such phenomena are often modeled in explicit

Hydrocode simulations. In Hydrocode simulations the numerical solution is obtained by an explicit time step calculation where the equation of state is combined with the constitutive material law [33] as a supplement equation to the equilibrium of mass, momentum and energy. A benefit of this technique is the consideration of shock waves in high-speed dynamic processes. The one-dimensional SHB experiments are simulated using the continuous Finite-Element technique to compare the assumptions of a macro-mechanical UHPC constitutive law. The model is subsequently used to develop and support a series of impact tests which were recently conducted and published in [34].

The parameters for the elasticity-, failure- and damage-surfaces (see Figure 13 and Equation (3)) in the stress-based material formulation for UHPC are taken from a literature review of recent quasi-static experiments [21, 25-28,29,35] calibrated for own quasi-static experiments which were conducted in parallel to the SHB tests using equivalent mixture and concreting. The UHPC model has a modular configuration based on the uniaxial stress strain relations under compression and tension. Based on this the commonly spread RHT concrete model for hydrocode simulations [36-41] is extended for fiber reinforced UHPC by the crack softening relation obtained in quasi-static tensile tests (fig. 5) using a simplified crack band width of $2 \cdot l_f$. The importance of this extension is emphasized by Leppänen in [41].

The strainrate effect observed in the SHB experiments is considered by using the modified CEB-formulation proposed by Malvar et al. [31] as the comparison with the experimental results show a satisfying accuracy for dynamic tensile strength. However only the first branch of the description is implemented in the constitutive law as physical effects of porous viscosity and mesomechanical failure could be confirmed indirectly by the UHPC SHB experiments as described in section 1 (Eq. (4)). For strainrates higher than $d\varepsilon/dt = 1s^{-1}$ the hydrocode simulation implicitly considers for local and nonlocal mass inertia effects

resulting in a delayed crack evolution at higher strainrates so that the second branch of the CEB formulation is obsolete as observed in [15].

$$f(p, \sigma_{eq}, \theta, \dot{\varepsilon}) = \sigma_{eq} - Y_{TXC}(p) R_3(\theta) F_{Rate}(\dot{\varepsilon}) = 0 \quad (3)$$

$$\frac{f_{t,dyn}}{f_{t,stat}} = \left(\frac{\dot{\varepsilon}}{\dot{\varepsilon}_0} \right)^\delta \quad (4)$$

$$\dot{\varepsilon}_0 = 10^{-6} \left[\frac{1}{s} \right], \delta = \frac{1}{1 + 8 \frac{f_c}{f_{c0}}}, \text{mit } f_{c0} = 10MPa$$

In addition to the three failure surface model large hydrostatic pressures are considered by an equation of state for UHPC. Hydrostatic compaction of concrete based materials can be described by a p- α -EOS in the pressure-density-energy relation (Eq. (5), (6)). UHPC is decomposed into the basic material sources to derive the p- α -EOS with the help of the Hugoniot Mixture Rule [42].

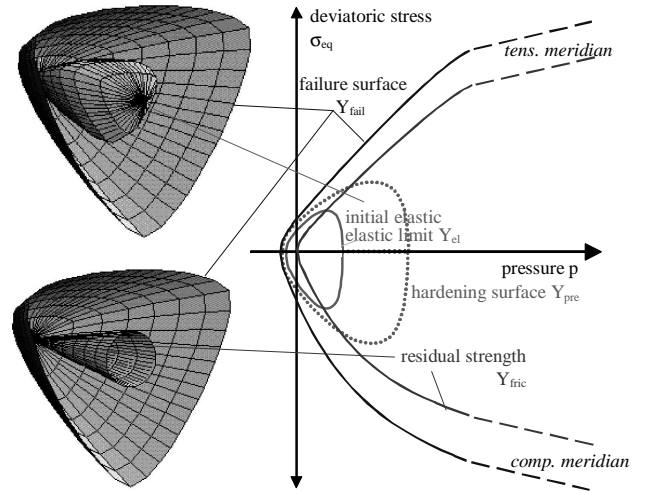


Figure 13: Three failure surfaces in the-RHT concrete model: Elasticity, Failure and Damage [34, 35]

$$p = f(\rho_{matrix}, e) \xrightarrow{\text{porous}} p = f(\rho\alpha, e) \quad (5)$$

$$\alpha = 1 + (\alpha_{init} - 1) \left[\frac{p_{comp} - p}{p_{comp} - p_{el}} \right]^N \quad (6)$$

4. NUMERICAL APPLICATION: FE-HYDROCODE SIMULATIONS

Hopkinson-Bar experiments

The calculation of the Split-Hopkinson-bar (SHB) experiments is performed with the measured speed constraints from the experiments, which can be determined from the strain measurement at the last measurement point on the input bar and the sound wave speed. The discretization is done with volume elements as 3-D cylinders with an element length of 5 mm.

The following illustrations (Figure 14) show as examples an experiment for a very brittle UHPC without fibers (left) and an experiment on a fiber-reinforced UHPC (right).

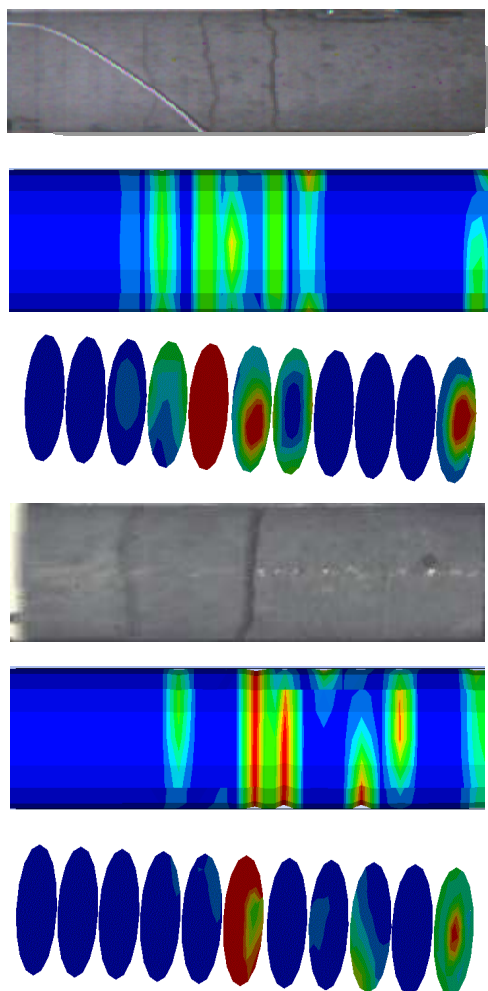


Figure 14: Numerical simulation results for Hopkinson-bar spallation experiments with the extended RHT-model for UHPC compared to the experimental results, loading direction from the left of the picture. [28]

Despite the relatively coarse and non-adaptive discretization – the element edge length of 5 mm is many times the crack opening – the element, in which the fracture occurs, can be clearly localized in both cases. For the pronounced multiple cracking of the brittle material without fibers (left), a Fourier analysis delivers information about the location of the initial crack, which is at the same location as in the segmented illustration calculated in Figure 14 (bottom).

Plate impact experiments

The comparison of predictive numerical simulations and scaled experimental investigations of rebar reinforced UHPC plates subjected to mechanical impact of aircraft engines [34,43] show a satisfying correlation (Figure 15). At a relevant aircraft impact velocity of 200 – 260 m/s a representative UHPC core segment shows only minor front side damage and rear side hairline cracks. The experiments 1,2 and 5 (Figure 15) have been conducted in this velocity regime. The ultimate loading capacity (ballistic limit) of the wall is reached at 320 m/s far higher than the maximum impact velocity. Please note that the bearing mechanism changes from the material's shear strength to the reinforcement membrane resistance as illustrated by the predictive numerical simulation and the experimental validation No. 3 respectively. Within this failure process large deformations occur before the material fails either in steel or concrete strain failure. A further increase of impact velocity finally leads to a perforation of the wall (Experiments No. 4, 6) with a residual velocity of the aircraft engine of 11 – 16m/s.

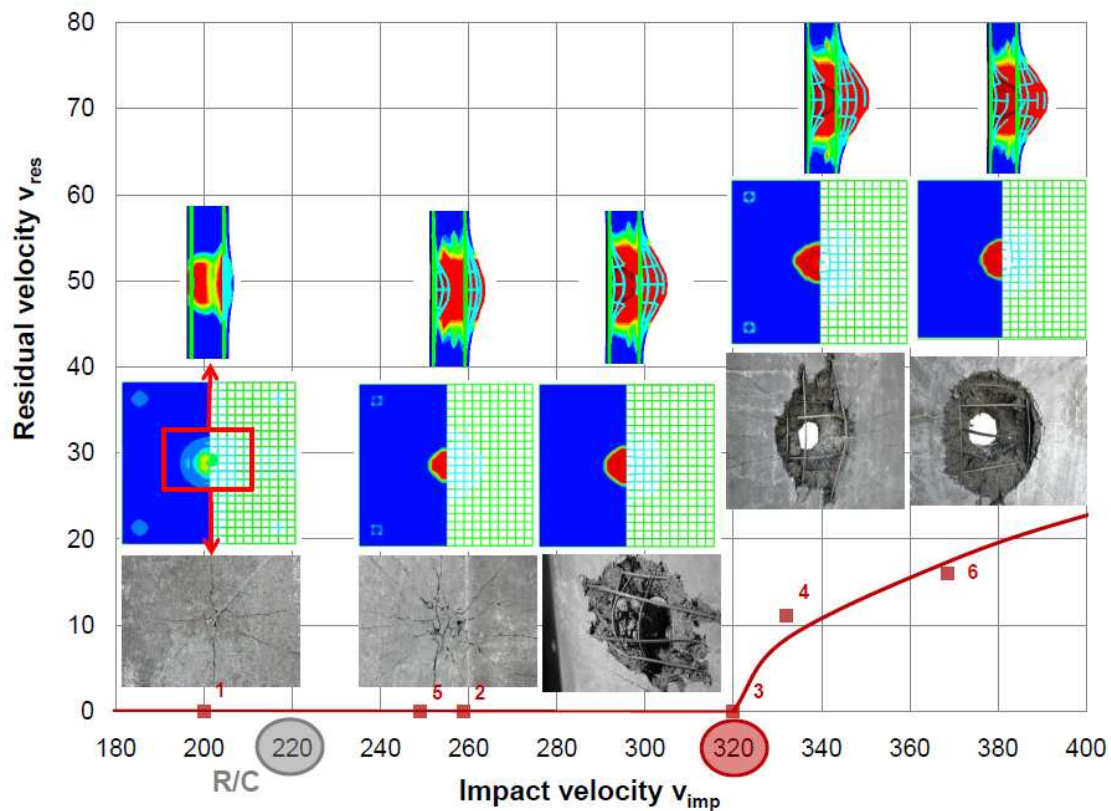


Figure 15: Numerical simulation results for UHPC plates subjected aircraft engine impact at different impact velocities [43]

CONCLUSION

The strainrate-effect observed for normal-strength concretes can be confirmed for the fiber reinforced Ultra-High-Performance Concrete by a series of Hopkinson-Bar spallation experiments. The significantly reduced amount of free water due to the low capillary porosity of the material leads to a reduced dynamic tension strength. Furthermore a comparison of fracture surfaces under static and dynamical failure shows a clear difference in failure to normal concrete where aggregates tend to fail with increasing loading rate. Both effects lead to a reduced dynamic increase factor for tension strength with increasing strength. For high strain rates however experimentally observed inertia effects in crack evolution still have the largest contribution to the macroscopic dynamic tension strength.

In a synthesis of the experimentally obtained static and dynamic tension strength, fracture energy, Young's modulus and fracture surfaces a stress-crack-opening relation is postulated and implemented in the RHT concrete Model. With the extension of this established concrete model by the obtained stress-crack-opening-damage-law Hopkinson-Bar experiments and more complex plate-impact experiments are simulated using FE-Hydrocode calculations. The good accuracy of the obtained results indicate that the dynamic tensile strength and the softening (damage) law are the most relevant fracture mechanical material properties for fiber reinforced UHPC at high strain rates.

REFERENCES

- [1] *Curbach, M.*: Festigkeitssteigerungen von Beton unter hohen Belastungsgeschwindigkeiten, Dissertation Universität Karlsruhe, 1987
- [2] *CEB-Comité Euro-international du Béton*: CEB FIP Model Code 1990, Bulletin d'information, No. 203-205, 1993
- [3] *Klepaczko, J.R.; Brara, A.*: An experimental method for dynamic tensile testing of concrete by spalling, *Int Journal of Impact Engineering* 25 (2001), 387-409
- [4] *Naaman, A.E.*: Fiber Reinforced Concrete under dynamic loading, SP 81-7, pp. 169-186
- [5] *Riedel, W.*: 10 Years of RHT: A review of concrete modeling and Hydrocode Application, pp. 143-165, in Hiermaier, S. (Ed.), *Predictive Modeling of Dynamic Processes-A Tribute to Klaus Thoma*, Springer, 2009
- [6] *Ross, C. A. et al.*: Moisture and strainrate effect on concrete strength. In: *ACI Materials Journal* 93 (1996) Heft 3, S. 293-300
- [7] *Schuler, H.*: Experimentelle und numerische Untersuchungen zur Schädigung von stoßbeanspruchtem Beton, Schriftenreihe ϵ - Fraunhofer Institut für Kurzezeitdynamik, EMI, Heft 6, 2004
- [8] *Schuler, H.*: Elemente der Werkstoffformulierung für Beton und deren Verwendung in der Kurzezeitdynamik, Beton- und Stahlbetonbau 102 (2007), Heft 11
- [9] *Schuler, H., Mayrhofer, C. Thoma, K.*: Spall experiments for the measurement of the tensile strength and fracture energy at high strain rates, *International Journal of the impact engineering* 32 (2006) 1635-1650
- [10] *Vegt, I.; Weerheijm, J.; Pedersen, R.R.; Sluys, L.J.*: Modeling of impact behavior of concrete – an experimental approach, In: *Computational modeling of concrete structures – EURO-C 2006*. 2006
- [11] *Lohrmann, G.*: Faserbeton unter hohen Dehngeschwindigkeiten; Dissertation. Instituts für Massivbau und Baustofftechnologie, Karlsruhe, 1998
- [12] *Lok, T.S., Zhao, P.J.*: Impact Response of SFRC using a Split-Hopkinson-Pressure-Bar, *Journal of Materials in Civil Engineering*, p.54-59, Jan/Feb 2004 ASCE
- [13] *Lok, T.S., Zhao, P.J., Lu, G.*: Using the Split Hopkinson-Bar to investigate dynamic behavior of SFRC, *Magazine of Concrete Research*, 2003, 55, No. 2, 183-191
- [14] *Suaris, W.; Shah, S.P.*: Strain rate effects in fiber reinforced concrete subjected to impact and impulsive loading, *Composites V13.*, No. 2, 1982, pp. 153-159
- [15] *Ozbolt, J.; Sharma, A.; Reinhardt, H.W.*: Dynamic fracture of concrete – compact tension specimen, *Int. Journ. Of Solids and Structures* 48, 2011, pp. 1534-1543
- [16] *Curbach, M.; Ortlepp, S.*: Untersuchungen an hochfestem Beton unter hohen Belastungsgeschwindigkeiten. In: *Beton- und Stahlbetonbau* 96 (2001) 4, S. 308
- [17] *Curbach, M.; Ortlepp, S.*: Research into high strength concrete at high rates of loading. Heft 3 der Schriftenreihe Baustoffe und Massivbau. Kassel : Kassel university press 2004, S. 461-470
- [18] *Ortlepp, S.*: Zur Beurteilung der Festigkeitssteigerung von hochfestem Beton unter hohen Dehngeschwindigkeiten, Dissertation, Universität Dresden 2006
- [19] *Schuler, H., Hansson, H.*: Fracture behavior of high Performance concrete (HPC) investigated with a Hopkinson-Bar, *Journal de Physique IV, France*, 134 (2006) 1145-1151, EDP Sciences
- [20] *Nöldgen, M.*: Modeling of Ultra High Performance Concrete (UHPC) under Impact Loading – Design of a High Rise Building Core against Aircraft Impact, Schriftenreihe ϵ Forschungsergebnisse aus der Kurzezeitdynamik, Fraunhofer Verlag, Heft 19, 2011, ISBN 978-3-8396-0286-7
- [21] *Schmidt, M. et al.*: Sachstandsbericht Ultrahochfester Beton, DAfStb Heft 561, Beuth Verlag 2008
- [22] *Rossi, P.*: A physical phenomenon which can explain the mechanical behaviour of concrete under high strain rates, *Materials and structures*, Vol. 24, S. 422-424, 1991
- [23] *Rossi, P.; van Mier J.G.M.; Boulay, C.; Le Malou, F.*: The dynamic behaviour of concrete: influence of free water, *Materials and structures*, Vol. 25, S. 509-514, 1992
- [24] *Fehling, E.; Schmidt, M.*: Entwicklung, Dauerhaftigkeit und Berechnung Ultra-Hochfester Betone (UHPC), Schriftenreihe Baustoffe und Massivbau Universität Kassel, Heft 1, 2005
- [25] *Leutbecher, T.; Fehling, E.*: Rissbildung und Zugtragverhalten von mit Stabstahl und Fasern bewehrtem Ultrahochfesten Beton (UHPC); Dissertation, Schriftenreihe Baustoffe und Massivbau, Heft 9, kassel university press GmbH, Kassel 2008.
- [26] *Leutbecher, T.; Fehling, E.*: Rissbildung und Zugtragverhalten von mit Fasern verstärktem Stahlbeton am Beispiel ultrahochfesten Betons, Teil 1: Rissmechanische Zusammenhänge, *Beton- und Stahlbetonbau* 104 (2009), Heft 6, S. 357-367
- [27] *Leutbecher, T.*: Rissbildung und Zugtragverhalten von mit Fasern verstärktem Stahlbeton am Beispiel ultrahochfesten Betons, Teil 2: Experimentelle Untersuchungen und Anwendungsbeispiele, *Beton- und Stahlbetonbau* 104 (2009), Heft 7, S. 406-415
- [28] *Nöldgen, M.; Millon, O.; Thoma, K.; Fehling, E.*: Hochdynamische Eigenschaften von Ultrahochleistungsbeton (UHPC), *Beton- und Stahlbetonbau* 104 (2009), Heft 11, Verlag Ernst & Sohn DOI 10.1002/best.200900038
- [29] *Millon, O., Nöldgen, M., Thoma, K., Riedel, W., Fehling E.*: Fiber-reinforced ultra-high performance concrete under tensile loads , (in press) *Journal de Physique IV* 2009
- [30] *Müller, H. S.; Curbach, M. et al.*: Constitutive modelling of high strength / high performance concrete – State-of-art report. *fib bulletin* 42, Lausanne, International Federation for Structural Concrete (fib), 2008
- [31] *Malvar, L.J.; Ross, C.A.*: Review of strain rate effects for concrete in tension, *ACI Materials Journal*, Title No. 95-M73, Nov-Dec 1998
- [32] *Pedersen, R.R.; Simone, A.; Sluys, L.J.*: An analysis of dynamic fracture in concrete with a continuum visco-elastic visco-plastic damage model,

- Engineering fracture mechanics 75 (2008) 3782-3805, Elsevier
- [33] *Riedel, W.*: Beton unter dynamischen Lasten: Meso- und makromechanische Modelle und ihre Parameter, Fraunhofer IRB Verlag 2004, ISBN 3-8167-6340-5
- [34] *Riedel, W.; Nöldgen, M.; Thoma, K.; Fehling, E.*, Local Damage to Ultra High Performance Concrete Structures caused by an Impact of Aircraft Engine Missiles, Nuclear Engineering and Design 240 (2010) pp. 2633-2642, DOI 10.1016/j.nucengdes.2010.07.036
- [35] *Riedel, W.; Kawai, N.; Kondo, K.*: Numerical assessment of impact strength measurements in concrete materials, International Journal of Impact Engineering 36 (2009), pp. 283-293
- [36] *Curbach, M.; Speck, K.*: Zweiachsiges Druckfestigkeit von UHPC, Beton- und Stahlbetonbau 10/2007, S.664-673
- [37] *Chen, W.F., Han D.J.*: Structural Plasticity, Prentice Hall, Englewood Cliffs, New Jersey, 1995
- [38] *Berg, V.S.; Preece, D.S.*: Reinforced Concrete Structures Failure Mechanisms Resulting from Explosive-induced Overpressures, Proceedings International society of Explosives Engineers, 2004G, Vol. 2
- [39] *Lu, Y.; Wang, Z.*: Characterization of structural effects from above ground explosion using coupled numerical simulation, Computers and Structures 84 (2006), pp. 1729
- [40] *Tham, C.Y.*: Reinforced Concrete Perforation and Penetration Simulation using AUTODYN 3D, Finite Element in Analysis and Design, 41 (2005), pp. 1401
- [41] *Leppänen, J.*: Concrete subjected to projectile and fragment impacts, Modeling of crack softening and strain rate dependency in tension, Int Journal of Impact Engineering 32 (2006), pp. 1828-1841
- [42] *Riedel, W., Wicklein, M.; Thoma, K.*: Shock Properties of Conventional and High Strength Concrete, Experimental and Mesomechanical Analysis, Int Journal of Impact Engineering 35/3 (2008), pp. 155-171
- [43] *Nöldgen, M.; Fehling, E.; Riedel, W.; Thoma K.*: Vulnerability and Robustness of a Security Skyscraper Subjected to Aircraft Impact, Computer-Aided Civil and Infrastructure Engineering, 27 (5), 2012, 358-368